2610588 Volumetric Fault Imaging based on Seismic Geometry Analysis

Haibin Di[1]; Ghassan AlRegib[1]
[1] Center for Energy and Geo Processing (CeGP), Georgia Institute of Technology, Atlanta, GA

ABSTRACT

Computer-aided fault imaging and interpretation is a fundamental tool for subsurface structure characterization and modeling, and the existing methods are primarily based on seismic discontinuity analysis (e.g., coherence and semblance) that evaluates the lateral variation of waveform and/or amplitude. However, such attributes have a limited resolution on subtle faults without apparent displacements in seismic images, which correspondingly decreases the accuracy of fault detection and interpretation. This study presents a new method for volumetric fault imaging based on seismic geometry analysis, consisting of two components. First, the curvature and flexure analysis is performed for fault detection from the perspective of evaluating the changes in the geometry of seismic reflectors, which helps highlight both the major faults and the subtle ones. Then an isolation operator is performed for differentiating the faults from the non-fault features observed in the curvature/flexure volumes, which leads to a fault volume with each lineament representing a potential fault. The added value of the proposed method is verified through applications to two 3D seismic volumes from the offshore New Zealand and the Netherlands North Sea. The results not only clearly depict the faulting complexities with varying sizes and orientations, but also indicates its great potential for improving the semiautomatic/automatic fault extraction from 3D seismic data.

INTRODUCTION

Robust characterization of faults and fractures is essential for subsurface structure interpretation from three-dimensional (3D) seismic surveying, and significant efforts have been devoted to computer-aided fault interpretation by quantifying seismic signals in various ways. Among them, the seismic discontinuity analysis was first presented as the coherence attribute for highlighting the faults and stratigraphic features from a seismic cube (Bahorich and Farmer, 1995), and since then, such attribute and its derivatives has been improved for better detection resolution and noise robustness (e.g., Luo et al., 1996; Marfurt et al., 1998; Gersztenkorn and Marfurt, 1999; Van Bemmel and Pepper, 2000; Cohen and Coifman, 2002; Tingdahl and de Rooij, 2005; Al-Dossary et al, 2014; Di and Gao, 2014a; Wang et al., 2016). However, besides the faults, the discontinuity analysis also highlights other non-fault features, such as salt domes and diapirs, stratigraphic channels, as well as coherent noises present in seismic data, all of which should be suppressed from the perspective of fault interpretation (Ashbridge et al., 2000; Barnes, 2006). To achieve such goal, Pedersen et al. (2002) introduce the concept of ant colony optimization from computer science and develop an ant-tracking algorithm for sharpening the lineaments in a variance volume. Al-BinHassan and Marfurt (2003) apply the 2D Hough transform for enhancing the fault lines on time slices, and later Wang and AlRegib (2014a) extend it to 3D space for fault surface detection from a semblance volume. Barnes (2006) performs eigenvector analysis to a coherence volume and designs a discontinuity filter for imaging the steeply-dipping discontinuities. Lavialle et al. (2006) present a nonlinear filtering approach for noise suppression and fault enhancement based on 3D gradient structure tensor (GST) analysis. Hale (2013) develops a discrete-scanning algorithm over dips and strikes for lineament thinning from a semblance volume. Zhang et al. (2014) binarize a discontinuity volume for fault skeletonization using a biometric algorithm. Machado et al. (2016) perform volumetric fault imaging by applying the directional Laplacian of a Gaussian (LoG) filter to coherence anomalies along reflector dip and azimuth. A comprehensive summary of the discontinuity analysis as well as the associated fault interpretation can be found in Chopra (2002), Kington (2015), and Di and Gao (2017).

However, the conventional discontinuity analysis is limited in its detection resolution for subtle faults and fractures beyond the seismic scale and more importantly offers no physical link for predicting the fundamental fracture properties (e.g., intensity, orientation, and sense of displacement) either quantitatively or qualitatively (Gao, 2013). Then for more robust fault detection and fracture characterization from 3D seismic data, the seismic geometry analysis is developed by quantifying the lateral changes in the geometry of seismic reflectors, including the second-order curvature (Roberts, 2001) and the third-order flexure attributes (Gao, 2013), with the former highlighting the tensile faults/fractures associated with reflector bending and the latter highlighting the shear faults/fractures associated with reflector shearing, respectively (Gao, 2013). In particular, for the curvature analysis, the Gaussian curvature was introduced to seismic interpretation from other industries and disciplines (e.g., Lisle, 1994), and various seismic curvatures have been developed for depicting subtle faults and fractures (Roberts, 2001; Al-Dossary and Marfurt, 2006). For the flexure analysis, the two-dimensional (2D) flexure was first computed as the lateral variation of the curvature attribute (Gao, 2013; Yu, 2014), and a set of algorithms extend the concept to 3D

space for volumetric flexure extraction (Di and Gao, 2014b, 2016a, 2016b; Gao and Di, 2015; Yu and Li, 2016). Comprehensive summaries of the curvature and flexure analysis can be found in Roberts (2001) and Di and Gao (2016c), respectively. With the enhanced resolution, the curvature and flexure analysis is capable of delineating the subtle lineaments that are often overlooked in the traditional discontinuity analysis, and thereby an experienced interpreter can manually pick the potential faults and from curvature/flexure maps. However, both attributes also reflect the variation of the reflection geometry over the anticlinal/synclinal blocks, and thereby such information is incorporated into the maps and adds the difficulties for computers/workstations to identify the faults in an automatic manner. For example, for a certain fault, the curvature attribute depicts its anticlinal and synclinal blocks, and zero curvature is estimated over the fault plane; the flexure attribute highlights the fault plane with a peak lineament and two sidelobes are observed over its blocks. Therefore, more work is expected for isolating the faults and fractures from the non-fault features, so that semi-automatic/automatic fault interpretation could be performed from the curvature/flexure volumes.

This paper presents a new method for fault interpretation based on the seismic geometry analysis. It starts with generating the curvature and flexure attributes from a seismic volume, both of which highlight the faults especially those with subtle geometry variations. Then two sets of operators are developed for isolating the faults from the curvature and flexure volumes, respectively. Finally, the added value of the proposed method is verified through applications to two seismic datasets over the Great South Basin (GSB) in offshore New Zealand and the F3 block in the Netherlands North Sea.

METHODOLOGY

The proposed method consists of two major components: seismic geometry analysis for highlighting the faults, and fault isolation for separating the faults from non-fault features. Both components are expanded in the section below. For the convenience of description, we use the vertical section of inline 504 from the F3 block dataset over the Netherlands North Sea, where the structure is dominated by salt domes as well as bending-induced faults over the anticline crest (Figure 1).

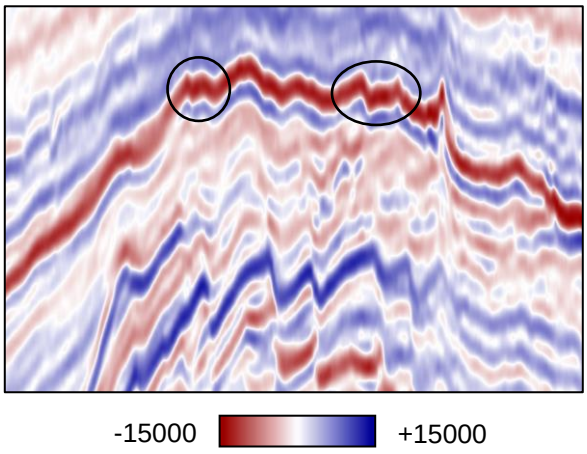

Figure 1. The vertical section of inline 504 from the F3 seismic dataset over the Netherlands North Sea used for illustrating the enhanced resolution of the proposed method on seismic fault interpretation, especially for the subtle ones without apparent displacements over the anticline crest (denoted by circles).

Seismic geometry analysis

Seismic geometry analysis, including the fist-order dip, the second-order curvature and the third-order flexure attributes, evaluates the lateral variation of the geometry of seismic reflectors in different scales and has been routinely used in subsurface structural interpretation. Compared to the traditional discontinuity analysis (e.g., coherence and variance) (Figure 2), it is superior in detecting the subtle faults without apparent displacement, such as those over the anticline crest in Figure 1. As shown in Figure 3, more lineaments could be recognized with the aid of the curvature and flexure attributes, especially the subtle ones not resolvable from the variance attribute (denoted by circles). Another improvement over the variance attribute is that, the curvature and flexure attributes have two properties, magnitude and azimuth, providing more geophysical implications for fault detection in a

quantitative manner. In particular, the former measures how the geometry of a reflector varies across faults, and correspondingly, the major faults with apparent displacement are represented as the lineaments of large curvature/flexure magnitude (Figure 3a and 3c). The azimuth property not only quantifies the most-likely orientation of faults in an automatic way, but also promotes the visibility of the subtle faults to the same level as the major ones, and correspondingly, the shadow effect of a major fault over its surrounding subtle faults is avoided, and the adjacent lineaments are better differentiated (Figure 3b and 3d). To be clear, among various curvatures and flexures, this study selects the signed maximum curvature and flexure that are considered most reasonable in geology and implements the analytical approach by Di and Gao (2016b) for computing these attributes.

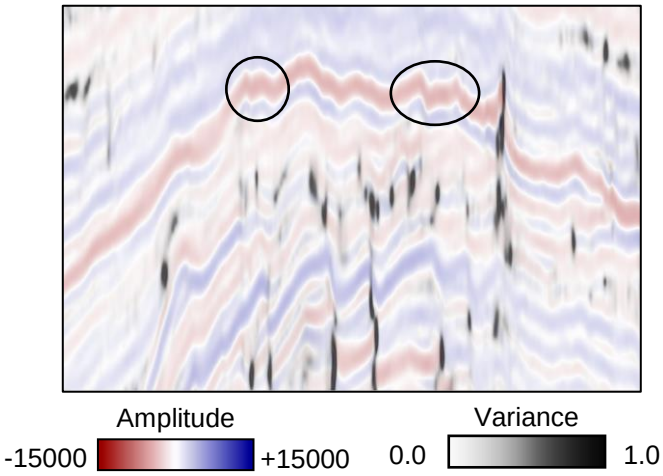

Figure 2. The variance attribute overlaying the seismic amplitude of inline 504 to demonstrate the limitation of the traditional discontinuity analysis on highlighting the subtle faults without apparent displacements over the anticline crest (denoted by circles).

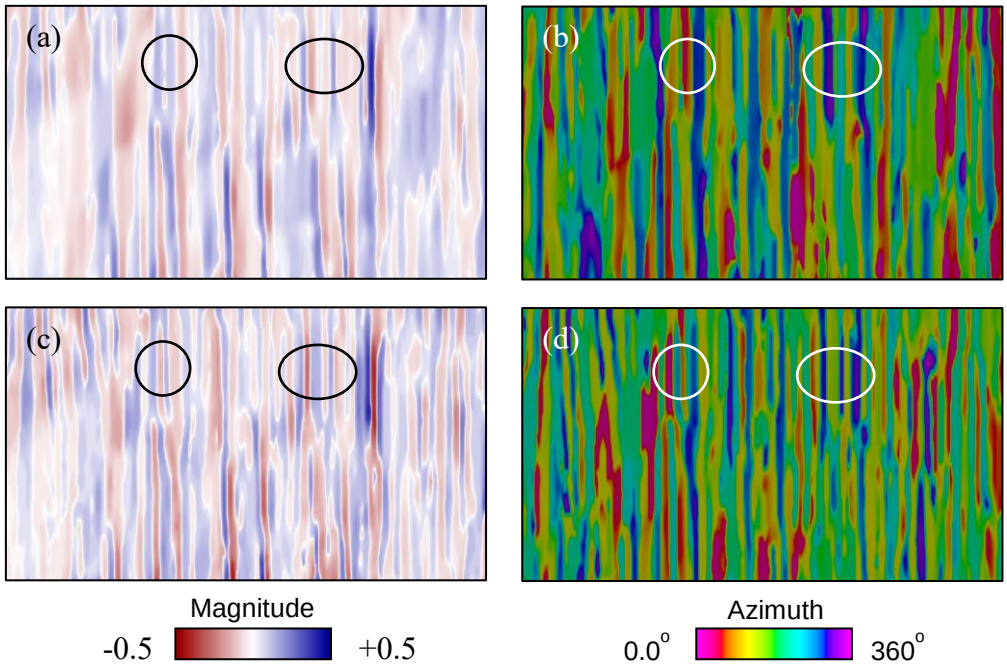

Figure 3. The geometric attributes of inline 504 to demonstrate the superiority of seismic geometry analysis in highlighting the subtle faults over the anticline crest (denoted by circles), including the magnitude (a) and azimuth (b) of the signed maximum curvature, and the magnitude (c) and azimuth (d) of the signed maximum flexure.

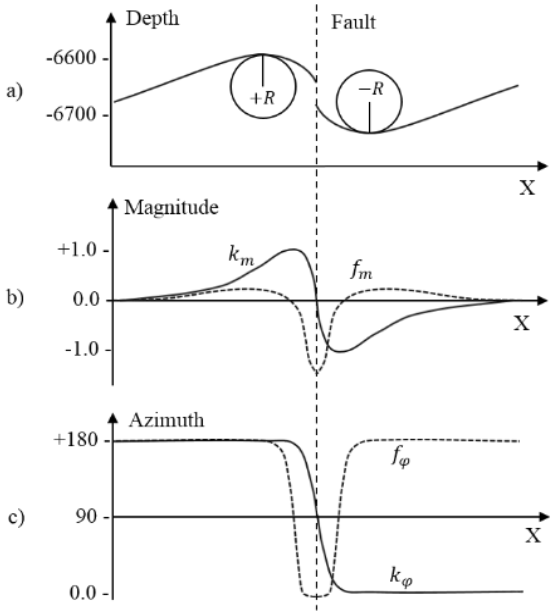

Figure 4. The sketch map for illustrating the different expressions of the curvature (solid curve) and flexure (dotted curve) attributes in highlighting a fault. R denotes the radius of the osculating circle tangent to the horizon.

Fault isolation

For fault interpretation from the curvature and flexure maps (Figure 3), it is necessary for understanding how a fault is represented by both attributes. Figure 4 builds a simple model for illustrating the differences, in which a simplified 2D horizon is cut by a fault. Specifically, using the magnitude property (Figure 4b), the fault is highlighted as a juxtaposition of positive curvature and negative curvature (denoted as solid curve), and their absolute values are similar or even the same over the fault blocks, whereas a negative peak with two positive sidelobes is observed for the fault by the flexure magnitude (denoted as dotted curve), and the ratio between the peak and the sidelobes is expected to vary from fault to fault, depending on the fault properties, such as dipping angle. For the azimuth property (Figure 4c), let the strike direction of the fault be 0°, the curvature azimuth is estimated as 0° at the synclinal block and jumps to the opposite direction (180°) at the anticlinal block (denoted as solid curve), whereas the flexure azimuth is estimated as 0° close to over the faulting zone but reverses (180°) at both blocks (denoted as dotted curve). To be clear, the curvature/flexure azimuth used in this study is extended to the range of [0°, 360°) by deliberately rotating the azimuth to its opposite direction when positive magnitude is estimated, so that the anticlinal and synclinal blocks could be differentiated for the convenience of fault interpretation.

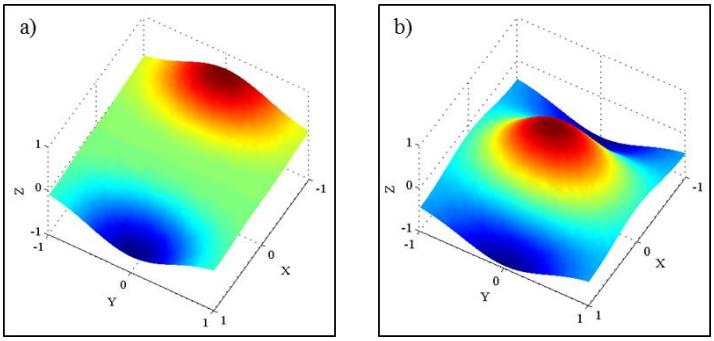

Figure 5. The operators used for fault isolation from the curvature (a) and flexure (b) attribute.

Then, we develop two isolation operators for separating faults from curvature and flexure attributes, respectively (Figure 5). In particular, the curvature operator represents the first derivative of the Gaussian filter and is capable of capturing the lateral variations of curvature over a fault (Figure 5a), whereas the flexure operator represents the

second derivative of the Gaussian filter and is capable of capturing the lateral variation of flexure over a fault (Figure 5b). Figure 6 and 7 display the fault maps by applying the proposed method to the vertical section in Figure 1.

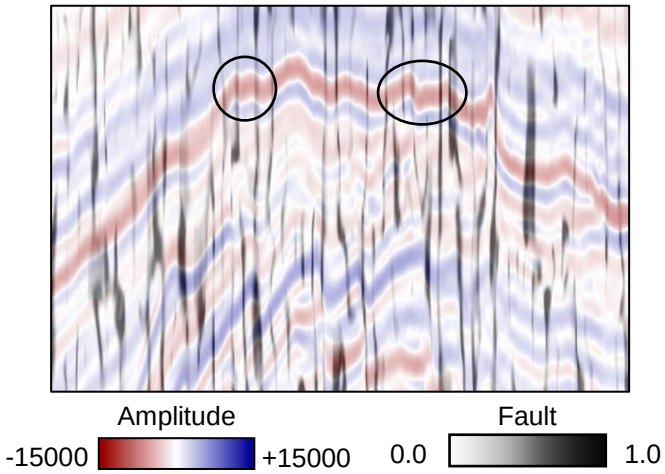

Figure 6. The fault map from the curvature attribute overlaying the seismic amplitude of inline 504. Note the enhanced imaging of both the major faults and the subtle ones over the anticlinal crest (denoted by circles), compared to the variance analysis (Figure 2).

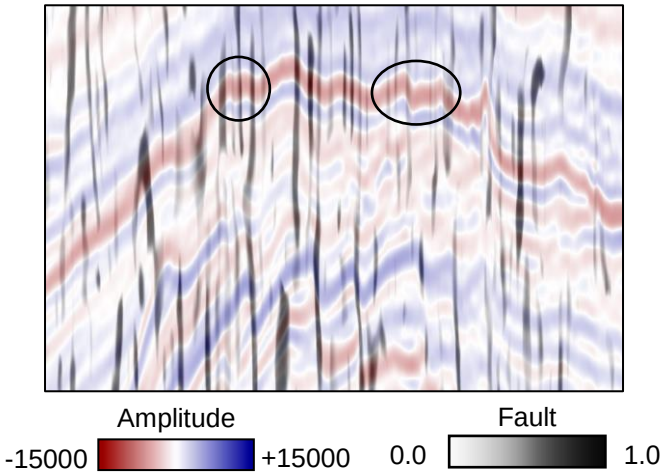

Figure 7. The fault map from the flexure attribute overlaying the seismic amplitude of inline 504. Note the enhanced imaging of both the major faults and the subtle ones over the anticlinal crest (denoted by circles), compared to the variance analysis (Figure 1).

APPLICATIONS

Following the description of the proposed method, we investigate its values through applications to two seismic datasets that are rich in faults, one from the Great South Basin (GSB) in offshore New Zealand and the other from the F3 bock in Netherlands North Sea. In general, the proposed method can assist fault interpretation from two perspectives, volumetric fault imaging and semiautomatic/automatic fault extraction.

Volumetric fault imaging

Volumetric fault imaging from 3D seismic data is a popular and efficient approach for fault interpretation, which not only allows interpreters to understand a fault system from the large scale, but also helps avoid the bias from manual interpretation, especially in the areas of faulting complexities with varying sizes and orientations. In such

case, the proposed method makes it possible for rapidly depicting an outline of the fault system in the subsurface, with an enhanced resolution compared to the conventional discontinuity analysis. Figure 8 displays the result from the GSB dataset, which was formed during the mid-Cretaceous and is rich in faults that cut the basin into several subbasins. Such volumetric fault imaging not only clearly demonstrates the spatial distribution of the polygonal faulting, but also makes it possible for interpreting every fault from the system and investigating its role in basin evolution over this area.

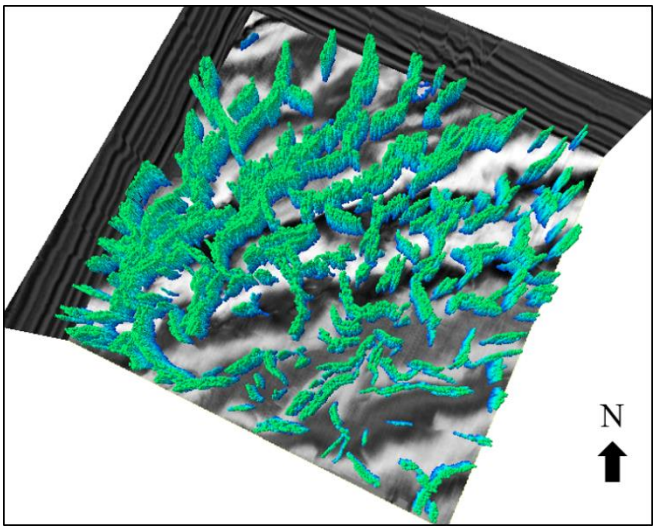

Figure 8. Volumetric fault imaging for the GSB seismic dataset from the fault volume generated by the proposed method.

Semiautomatic/automatic fault extraction

Besides the volumetric fault imaging, the fault volume generated by the proposed method can also be used for fault extraction in a semiautomatic/automatic manner to serve quantitative structural framework modeling. Take seeded fault picking for example. Figure 9 displays the extracted fault patches from the F3 dataset in 3D view, and for quality control, we then clip them to two sections (Figure 10), with each black line representing one fault. Both maps demonstrate good matches between the fault patches and the original seismic images, indicating the accuracy of the proposed method in guiding fault extraction.

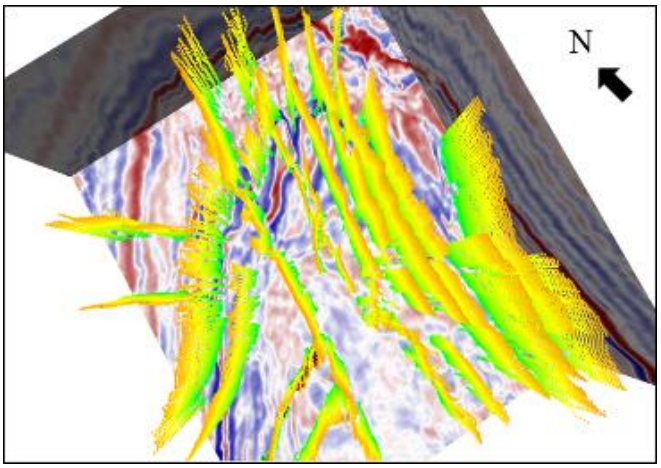

Figure 9. 3D view of the fault patches extracted in the F3 seismic dataset from the fault volume generated by the proposed method.

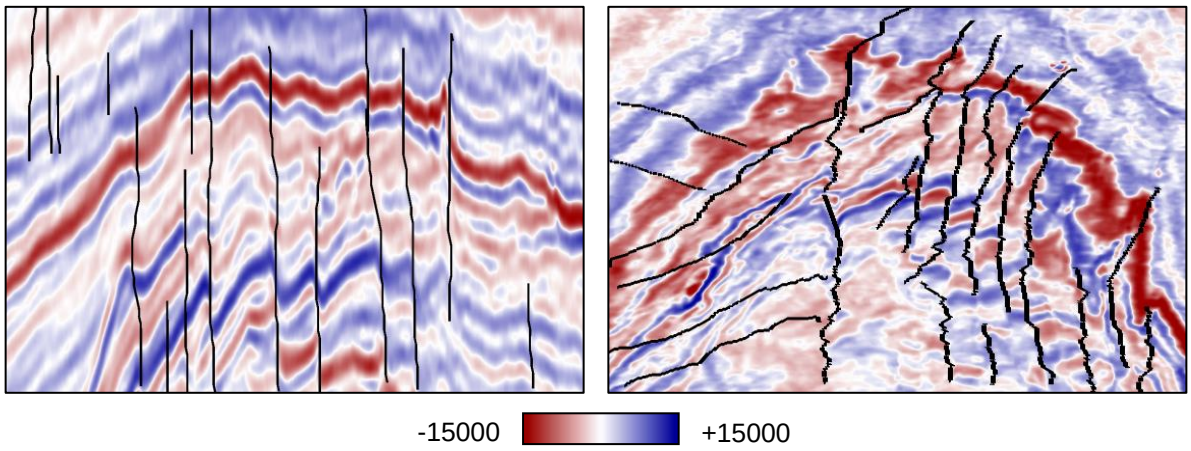

Figure 10. The clipping of the extracted fault patches in Figure 9 to two sections. Note the good match between the pickings and the seismic image.

CONCLUSIONS

We have presented a new method for faults detection and interpretation from 3D seismic data that consists of two major components. First, the seismic geometry analysis is performed to highlight both the major faults and the subtle ones, especially those often overlooked in the traditional discontinuity analysis. Then, an isolation operator is applied to separate the potential faults from the non-fault features and provide a fault volume for advanced fault interpretation. With the assistance of the proposed method, a fault system can be better investigated in two stages: first to perform volumetric fault imaging for depicting its spatial distribution and investigating its role in geologic deformation, and second to pick the target faults as patches for quantitative structure interpretation and framework modeling.

ACKNOWLEDGMENTS

This work is supported by the Center for Energy and Geo Processing at Georgia Tech and King Fahd University of Petroleum and Minerals. We thank the OpendTect Open Seismic Repository (opendtect.org/osr) for providing the F3 dataset over the Netherlands North Sea, and the New Zealand Petroleum and Minerals (NZP&M) for the GSB dataset.

REFERENCES

Al-BinHassan, N. M., and K. J. Marfurt, 2003, Fault detection using Hough transforms: 83rd Annual International Meeting, SEG, Expanded Abstracts, 1719-1721.

Al-Dossary, S., and K. J. Marfurt, 2006, 3D volumetric multispectral estimates of reflector curvature and rotation: Geophysics, 71, 41-51.

Al-Dossary, S., Y. E. Wang, and M. McFarlane, 2014, Estimating randomness using seismic disorder: Interpretation, 2, SA93-SA97.

Ashbridge, J., F. Coutel, M. Welch, and C. Pryce, 2000, Fault and fracture prediction from coherence data analysis: 70th Annual Intermeeting, SEG, Expanded Abstracts, 1564-1567.

Bahorich, M., and S. Farmer, 1995, 3-D seismic coherency for faults and stratigraphic features: The Leading Edge, 14, 1053-1058.

Barnes, A., 2006, A filter to improve seismic discontinuity data for fault interpretation: Geophysics, 71, P1-P4.

Chopra, S., 2002, Coherence cube and beyond: First Break, 20, 27-33.

Cohen, I., and R. R. Coifman, 2002, Local discontinuity measures for 3-D seismic data: Geophysics, 67, 1933-1945.

Di, H., and D. Gao, 2014a, Gray-level transformation and Canny edge detection for 3D seismic discontinuity enhancement: Computers & Geosciences, 72, 192-200.

Di, H., and D. Gao, 2014b, A new algorithm for evaluating 3D curvature and curvature gradient from improved fracture detection: Computer & Geosciences, 70, 15-25.

Di, H., and D. Gao, 2016a, Volumetric extraction of most positive/negative curvature and flexure attributes for improved fracture characterization from 3D seismic data: Geophysical Prospecting, 64, 1454-1468.
Di, H., and D. Gao, 2016b, Improved estimates of seismic curvature and flexure based on 3D surface rotation in the presence of structure dip: Geophysics, 81, IM37-IM47.
Di, H., and D. Gao, 2016c, 3D seismic flexure analysis for subsurface fault detection and fracture characterization: Pure and Applied Geophysics, doi: 10.1007/s00024-016-1406-9.
Di, H., and D. Gao, 2017, Seismic attribute-aided fault detection in petroleum industry: A review: in Daniel Martion (eds), Fault detection: Methods, Applications and Technology, 53-80.
Gao, D., 2013, Integrating 3D seismic curvature and curvature gradient attributes for fracture detection: Methodologies and Interpretational implications: Geophysics, 78, O21-O38.
Gao, D., and H. Di, 2015, Extreme curvature and extreme flexure analysis for fracture characterization from 3D seismic data: New analytical workflows and geologic implications: Geophysics, 80, IM11-IM20.
Gersztenkorn, A., and K. J. Marfurt, 1999, Eigenstructure-based coherence computations as an aid to 3-D structural and stratigraphic mapping: Geophysics, 64, 1468-1479.
Hale, D., 2013, Methods to compute fault images, extract fault surfaces, and estimate fault throws from 3D seismic images. Geophysics, 78, O33-O43.
Kington, J., 2015, Semblance, coherence, and other discontinuity attributes: The Leading Edge, 34, 1510-1512.
Lavialle, O., S. Pop, C. Germain, M. Donias, S. Guillon, N. Keskes, and Y. Berthoumieu, 2006, Seismic fault preserving diffusion: Journal of Applied Geophysics, 61, 132-141.
Lisle, R. J., 1994, Detection of zones of abnormal strains in structures using Gaussian curvature analysis: AAPG Bulletin, 78, 1811-1819.
Luo, Y., W. G. Higgs, and W. S. Kowalik, 1996, Edge detection and stratigraphic analysis using 3-D seismic data: 66th Annual International Meeting, SEG, Expanded Abstracts, 324-327.
Machado, G., A. Alali, B. Hutchinson, O. Olorunsola, K. J. Marfurt, 2016, Display and enhancement of volumetric fault images: Interpretation, 4, SB51-SB61.
Marfurt, K. J., R. L. Kirlin, S. L. Farmer, and M. S. Bahorich, 1998, 3-D seismic attributes using a semblance-based coherency algorithm: Geophysics, 63, 1150-1165.
Pedersen, S. I., T. Randen, L. Sonneland, and O. Steen, 2002, Automatic fault extraction using artificial ants: 72nd Annual International Meeting, SEG, Expanded Abstracts, 512-515.
Roberts, A., 2001, Curvature attributes and their application to 3D interpreted horizons: First break, 19, 85-100.
Tingdahl, K. M., and M. de Rooij, 2005, Semi-automatic detection of faults in 3D seismic data: Geophysical Prospecting, 53, 533-542.
Van Bemmel, P. P., and R. E. F. Pepper, 2000, Seismic signal processing method and apparatus for generating a cube of variance values: U. S. Patent 6,151,555.
Wang, S., S. Yuan, B. Yan, Y. He, and W. Sun, 2016, Directional complex-valued coherence attribute for discontinuous edge detection: Journal of Applied Geophysics, 129, 1-7.
Yu, J., 2014, Using cylindrical surface-based curvature change rate to detect faults and fractures: Geophysics, 79, O1-O9.
Yu, J., and L. Zhong, 2016, Arctangent function-based third derivative attribute for characterization of faults: Geophysical Prospecting, doi: 10.1111/1365-2478.12462.
Zhang, B., Y. Liu, M. Pelissier, and N. Hemstra, 2014, Semiautomated fault interpretation based on seismic attributes: Interpretation, 2, SA11-SA19.